Electronic Supplementary Information (ESI)

Room-Temperature Synthesis of a Fluorine-Rich Nanoporous Organic Polymer with Hierarchical Porosity for Selective Separation of Fluorinated Greenhouse Gases

Qilin Wang,[a] Jiangli Zhu,[a] and Jun Yan.[a, b,*]

[a]*School of Materials Science and Engineering, North Minzu University, Yinchuan 750021, China*，

[b]*Institute of Functional and Structural Characteristic Materials, Helanshan Laboratory, Yinchuan 750021, China*

Corresponding Authors:

*Email: yanjun2018@nun.edu.cn (Jun Yan)；

Contents

Experimental section

Materials

2,3,4,5,6-pentafluorobenzaldehyde (97%), 4,4′,4″-tris(9H-carbazol-9-yl)triphenylamine (98%), trifluoromethanesulfonic acid (98%), tetrahydrofuran (THF, 99.5%), dichloromethane (DCM, 99.8%), dimethyl sulfoxide (DMSO, 99.9%), and N,N-dimethylformamide (DMF, 99.9%) were purchased from commercial suppliers (Macklin) and used as received without further purification unless otherwise noted.

Synthesis of CNOP-13

Under a nitrogen atmosphere, a dry 50 mL Schlenk flask was charged with 2, 3, 4, 5, 6-pentafluorobenzaldehyde (0.29 g, 1.5 mmol), 4, 4', 4''-tris(9H-carbazol-9-yl)triphenylamine (0.37 g, 0.5 mmol), and dichloromethane (13.2 mL). The mixture was stirred at room temperature for 30 min, followed by the dropwise addition of trifluoromethanesulfonic acid (290 μL, 3.3 mmol) over a period of 20 min. After stirring for an additional 12 h at room temperature, the resulting precipitate was collected by vacuum filtration and washed successively with DMF, DMSO, and THF. The crude solid was further purified via Soxhlet extraction with THF for 3 days and dried under vacuum at 120℃ for 48 h to afford CNOP-13 as a brown powder (99% yield).

Characterization

Field-emission scanning electron microscopy (FE-SEM; ZEISS SUPRA™ 55) was utilized to visualize the morphology of CNOP-13, while its crystalline nature was assessed via powder X-ray diffraction (PXRD) on a Rigaku D/Max-2400 system (Cu Kα source, 40 kV, 200 mA) scanning at $2°\cdot min^{-1}$. Thermal stability was characterized using a TA Instruments Q50 analyzer (under N_2 flow, ramping 10 $°C\cdot min^{-1}$ to 800 °C). Comprehensive structural analysis of CNOP-13 was performed

using solid-state ^{13}C CP/TOSS NMR spectroscopy (Bruker AVANCE III HD 600 MHz), Fourier transform infrared (FTIR) spectroscopy (Thermo Fisher Scientific Nicolet™ 20XB), and X-ray photoelectron spectroscopy (XPS, Thermo Scientific K-Alpha with Al K α source). For porosity analysis, N_2 sorption isotherms at 77 K were acquired on a Quantachrome Autosorb iQ3 after vacuum-degassing the samples at 120℃ for 12 h. A BSD-PMC analyzer (BeiShiDe Instrument) was employed to measure single-component isotherms of N_2, SF_6, and CF_4 at 273 and 298 K. Based on the single-site Langmuir-Freundlich fitting of these isotherms, Ideal Adsorbed Solution Theory (IAST) selectivities were calculated for binary mixtures (SF_6/N_2 and CF_4/N_2, 10:90 v/v). Dynamic separation performance was evaluated in a fixed-bed quartz column (0.6 cm ID × 7.5 cm L) loaded with 0.50 g of CNOP-13. The sample was activated at 373 K under He flow (40 mL min^{-1}) for 3 h. Subsequently, a gas mixture of SF_6/N_2 (10/90 v/v) was fed at 20 mL min^{-1} (298 K, 1 bar). The effluent was analyzed in real-time using a Pfeiffer Vacuum ThermoStar mass spectrometer by tracking ion signals at m/z 89 (SF_3^+) and 28 (N_2^+). Analogous tests were conducted for CF_4/N_2 mixtures (monitoring m/z 69 for CF_3^+), and adsorption capacities were derived by integrating the resulting breakthrough curves.

Ideal Adsorbed Solution Theory (IAST) Selectivity

The pure component isotherms of SF_6, CF_4, and N_2 were fitted with the single-site Langmuir (SSL) model.

$$N = \frac{A \times B \times P^c}{1 + B \times P^c} \quad \text{S1}$$

Where N is molar loading of adsorbate (mmol/g), P is pressure (kPa), A is saturation loading (mmol/g), B is a parameter in the pure component Langmuir isotherm (kPa^{-1}), C is the parameter of Langmuir-Freundlich.

Pure-component isotherm fitting parameters were then used for calculating Ideal Adsorbed Solution Theory (IAST)[1] binary-gas adsorption selectivities, S, defined as

$$S = \frac{q_1/q_2}{P_1/P_2} \quad \text{S2}$$

In the equation, q_1 and q_2 are the molar loadings in the adsorbed phase in equilibrium with the bulk gas phase with partial pressures p_1 and p_2.

Computational Details

The geometric structures of CNOP-13 were fully optimized via density functional theory (DFT) calculations, as implemented in the DMol3 module of Materials Studio software. These optimizations utilized the Perdew-Burke-Ernzerhof (PBE) exchange-correlation functional within the generalized gradient approximation (GGA) framework, providing a robust description of the electronic structure and molecular geometry. To elucidate charge distribution patterns and identify prospective adsorption sites, molecular electrostatic potential (ESP) surfaces were generated by projecting the ESP onto the electron density isosurface of optimized fragments from CNOP-13. The ESP, which quantifies the potential energy of a unit positive test charge at any spatial point, serves as a powerful tool for visualizing regions prone to electrophilic interactions (negative ESP) or nucleophilic attacks (positive ESP), thereby guiding predictions of molecular reactivity.

Adsorption energies (ΔE_{ads}) for the guest molecules (SF_6, CF_4, and N_2) on CNOP-13 were evaluated using the Forcite module in Materials Studio. Initial geometry optimizations of the isolated adsorbates and host polymer were conducted with the Universal Force Field (UFF). Subsequently, composite structures comprising the adsorbate and CNOP-13 were assembled and further optimized under UFF constraints. The adsorption energy was then derived from single-point energy evaluations, also employing UFF, according to the formula:

$$\boldsymbol{\Delta E_{ads}=E_{complex}-(E_{host}+E_{guest})} \quad \text{S3}$$

Here, ΔE_{ads} denotes the adsorption energy, while $E_{complex}$, E_{guest} and E_{host} represent the total energies of the adsorbate-polymer complex, the isolated polymer, and the isolated gas molecule, respectively. This approach yields a quantitative measure of binding affinity, accounting for van der Waals and electrostatic contributions in a computationally efficient manner.

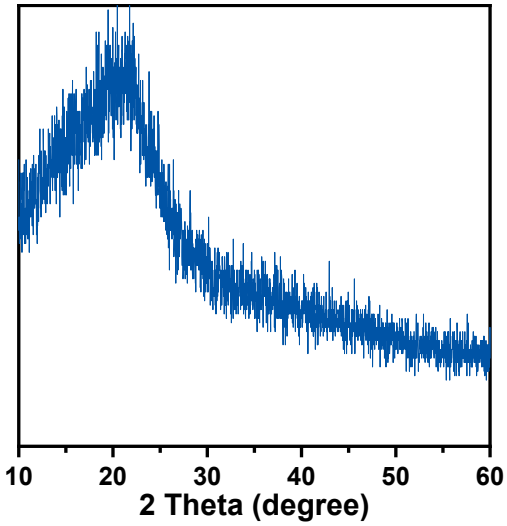

Figure S1. Wide-angle X-ray diffraction of CNOP-13..

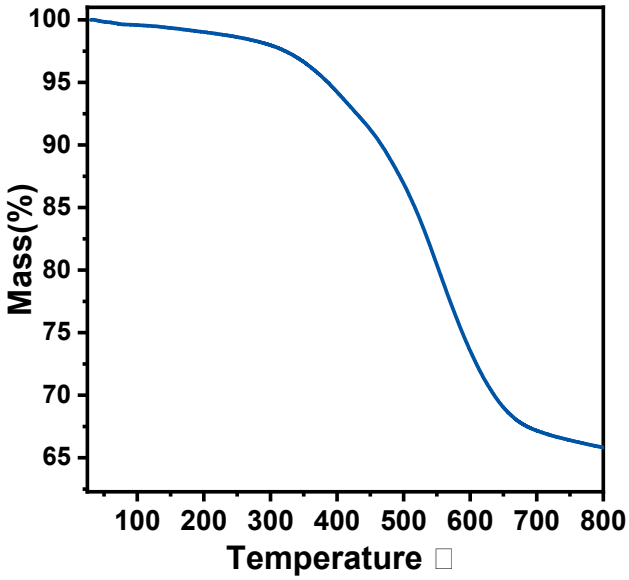

Figure S2. TGA curve of CNOP-13.

Figure S3. The SEM image of CNOP-13.

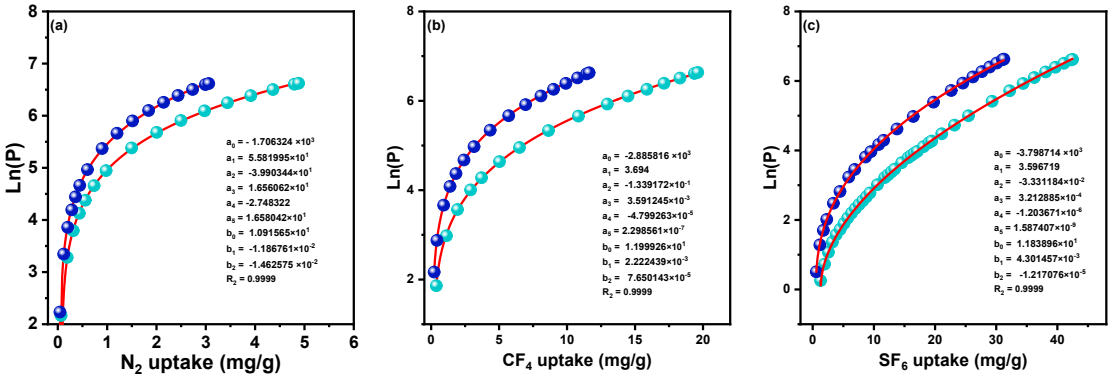

Figure S4. Virial equation fitting of N_2(a), CF_4 (b), and SF_6 (c) adsorption isotherms of CNOP-13.

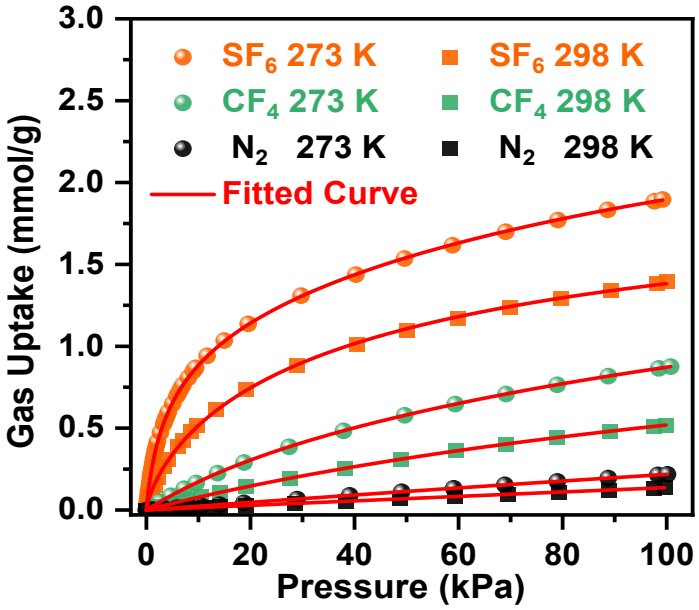

Figure S5. Adsorption isotherms and single-site Langmuir−Freundlich fitting curves for SF_6, CF_4, and N_2 on CNOP-13 at 273 K and 298 K.

Figure S6. Electrostatic potential (ESP) map of the CNOP-13.

Table S1. Single-site Langmuir-Freundlich fitting parameters for CNOP-13.

Sample	T/K	Gas	A(mmol/g)	B(kPa^{-C})	C	R^2
CNOP-13	273K	SF_6	2.7753	1.0475×10^{-1}	0.6453	0.9987
		CF_4	1.9514	1.1598×10^{-2}	0.9206	0.9999
		N_2	2.7791	8.5875×10^{-4}	0.9974	0.9999
	298 K	SF_6	2.1920	5.5473×10^{-2}	0.7442	0.9996
		CF_4	1.5360	5.5887×10^{-3}	0.9803	0.9999
		N_2	1.6703	7.7883×10^{-4}	1.0287	0.9999

Table S2. SF_6 adsorption capacities and N_2 Selectivities of CNOP-13 and some reported porous organic polymers at 100 kPa.

Materials	S_{BET} ($m^2\ g^{-1}$)	SF_6 uptake (mmol g^{-1})		SF_6/N_2 (10:90)		Ref.
		273 K	298 K	273 K	298 K	
CNOP-13	762	1.90	1.40	92.2	65.1	This work
CNOP-7	1270	2.60	1.90	108	73	[2]
ANOP-8	694	1.25	0.92	80	65	[3]
NMUCOF-1	991	1.76	1.11	41	37	[4]
RCOF-2	763	2.41	1.86	70	45	[5]
RCOF-3	242	0.91	0.58	34	25	[5]
RCOF-1–5	428	1.14	1.11	72	52	[5]
COF300	1106	4.03	3.09	70	51	[5]
FCOF-1	1885	2.21	1.08	22	14	[6]
KFCOF-1	744	1.58	0.99	42	33	[6]
SNNU-202	1319	-	4.94	-	9	[7]
SNNU-203	1522	-	5.6	-	27	[7]
SNNU-204	2170	-	6.06	-	49	[7]
ZIF-7	396	-	0.46	-	22[b]	[8]
BrCOF-2	1602	-	~1.3	-	17	[9]
BrCOF-2-CF_3	1514	-	1.45	-	39	[9]
PAF-XJTU-4	1419	-	3.34	-	29	[10]
TNOP-1	822	2.08	1.59	95	84	[11]
TNOP-2	605	1.12	0.92	83	77	[12]
POPTrB-4F	775	2.88	-	-	62[a]	[13]
POPTrB-8F	628	2.21	-	-	51[a]	[13]
PKAN-1	977	2.97	2.40	-	113	[14]
Ppy-POF	641	-	0.84	-	74	[15]
PAF-4F	1071	2.46	-	-	38[a]	[16]

[a]SF_6/N_2=1:99; [b]IAST selectivity in 293 K;

Reference

1. A. P. Myers, J. M., AlChE J, 1965, 11, 7.

2. S. Tong, L. Yao, Q. Wang, J. Zhu, Z. Wang and J. Yan, *ACS Macro Lett.* , 2024, **13**, 1469-1475.

3. J. Zhu, D. Luo, Q. Wang, S. Tong, Z. Wang and J. Yan, *Chem. Commun.*, 2024, **60**, 12209-12212.

4. J. Zhu, Q. Wang, Z. Wang and J. Yan, *ACS Appl. Polym. Mater.* , 2025, **7**, 9488-9495.

5. Q. Liao, H. Xu, C. Ke, Y. Zhang, Q. Han, Y. Zhang, Y. Xu, D. Wang and K. Xi, *Sep. Purif. Technol.*, 2023, **306**, 122595.

6. X. Sun, L. Zhou, J. Chen, Z. Jia, Z. Zhao and Z. Zhao, *J. Mater. Chem. A*, 2025, **13**, 2360-2377.

7. Y.-P. Li, J.-J. Ni, S. Li, J. Wang, Z.-Y. Sui and X.-F. Xu, *Journal of Solid State Chemistry*, 2024, **329**, 124443.

8. M. Åhlén, A. Jaworski, M. Strømme and O. Cheung, *Chem. Eng. J.*, 2021, **422**, 130117.

9. Q. Liao, C. Ke, X. Huang, D. Wang, Q. Han, Y. Zhang, Y. Zhang and K. Xi, *Angew. Chem. Int. Ed.*, 2020, **60**, 1411-1416.

10. Y. Wu, X. Li, Y. Li, C. Tao, Y. Tang, S. Wang, Y. Fu, W. Ma, W. Zhang and H. Ma, *Sep. Purif. Technol.*, 2023, **315**, 123657.

11. X. Yang, Q. Wang, J. Zhu, J. Yan and S. Guo, *ACS Materials Letters*, 2025, **7**, 1940-1946.

12. J. Zhu, X. Chen, Q. Wang and J. Yan, *ACS Appl. Mater. Interfaces* , 2025, **17**, 70029-70038.

13. W. Zhang, Y. Wu, Y. Li, S. Chen, Y. Fu, Z. Zhang, T. Yan, S. Wang and H. Ma, *Macromolecules*, 2022, **55**, 1435-1444.

14. Q. Wang, J. Zhu and J. Yan, *ACS Macro Lett.* , 2025, **14**, 1535-1542.

15. W. Zhang, Y. Li, Y. Wu, W. Huang, S. Wang, Y. Fu, W. Ma, X. Li and H. Ma, *ACS Appl. Mater. Interfaces* , 2023, **15**, 29468-29477.

16. W. Zhang, Y. Li, S. Wang, Y. Wu, S. Chen, Y. Fu, W. Ma, Z. Zhang and H. Ma, *ACS Appl. Mater. Interfaces* , 2022, **14**, 35126-35137.